

Study of Diboson Production at CMS

Kalanand Mishra

Fermi National Accelerator Laboratory, Batavia, IL 60510, USA

I present an overview of the measurements of the diboson (WW , WZ , ZZ , $W\gamma$, and $Z\gamma$) production cross sections in proton-proton collisions at $\sqrt{s} = 7$ TeV. The measurements are based on 36 pb^{-1} and 1.1 fb^{-1} of data collected with the CMS detector at the LHC in 2010 and 2011, respectively. The vector bosons W and Z are reconstructed in purely leptonic decays. The measured cross sections are compared with the Standard Model expectations calculated at next-to-leading order in perturbative QCD. Limits on anomalous triple gauge boson couplings are derived.

1. Introduction

The gauge boson self-interactions appear as vertices involving three or four gauge bosons. The study of diboson production in proton-proton collisions is an important test of the standard model (SM) because of its sensitivity to the self-interaction between gauge bosons via trilinear gauge couplings (TGC). The values of these couplings are fully fixed in the SM by the gauge structure of the $SU(2) \times U(1)$ Lagrangian. Any deviation, manifested as an increased cross section, would indicate new physics. Understanding diboson production is also important for Higgs boson searches, because electroweak WW and ZZ production are irreducible backgrounds for high mass Higgs.

2. CMS Detector

A detailed description of the CMS detector can be found elsewhere [1]. The layout comprises a superconducting solenoid providing a uniform magnetic field of 3.8 T. The bore of the solenoid is instrumented with various particle detection systems. The inner tracking system is composed of a pixel detector with three barrel layers at radii between 4.4 and 10.2 cm and a silicon strip tracker with 10 barrel detection layers extending outwards to a radius of 1.1 m. Each system is completed by two end caps, extending the acceptance up to $|\eta| < 2.5$. A lead tungstate crystal electromagnetic calorimeter with fine transverse ($\Delta\eta, \Delta\phi$) granularity and a brass-scintillator hadronic calorimeter surround the tracking volume and cover the region $|\eta| < 3$. The steel return yoke outside the solenoid is in turn instrumented with gas detectors which are used to identify muons in the range $|\eta| < 2.4$. The barrel region is covered by drift tube chambers and the end cap region by cathode strip chambers, each complemented by resistive plate chambers.

3. Measurement of the $WW \rightarrow \ell^+ \nu \ell^- \bar{\nu}$ cross section

This measurement is based on data taken in 2011 corresponding to an integrated luminosity (\mathcal{L}) of 1.1 fb^{-1} . A similar analysis using 35 pb^{-1} of 2010 data is described in Ref. [2]. The fully leptonic W^+W^- final state consists of two oppositely charged leptons and large missing energy from the two undetectable neutrinos. Events are selected using triggers that require the presence of one or two high- p_T leptons (electrons or muons). Lepton candidates are then reconstructed offline and events with two oppositely charged, high- p_T , isolated leptons (ee , $\mu\mu$, $e\mu$) are chosen using the following criteria:

- Leading lepton $p_T > 20 \text{ GeV}$, second lepton $p_T > 10 \text{ GeV}$.
- To reject Drell-Yan events with mismeasured E_T^{miss} associated with poorly reconstructed leptons, we use the *projected* E_T^{miss} which is the component of E_T^{miss} transverse to the closest lepton if $\Delta\phi(\ell, E_T^{\text{miss}}) < \pi/2$, and the full E_T^{miss} otherwise. Events are required to have *projected* E_T^{miss} above 40 GeV in the e^+e^- and $\mu^+\mu^-$ final states, and above 20 GeV for the $e^\pm\mu^\mp$ final state. These requirements remove more than 99% of the Drell-Yan background.
- To further minimize the Drell-Yan background, events with same flavor leptons with a dilepton invariant mass within $\pm 15 \text{ GeV}$ of the Z mass are rejected. Also for this final state, require $\Delta\phi(\text{dilepton, jet}) < 165^\circ$ for the most energetic jet with $p_T > 15 \text{ GeV}$ to cope with the $Z+1$ jet background.

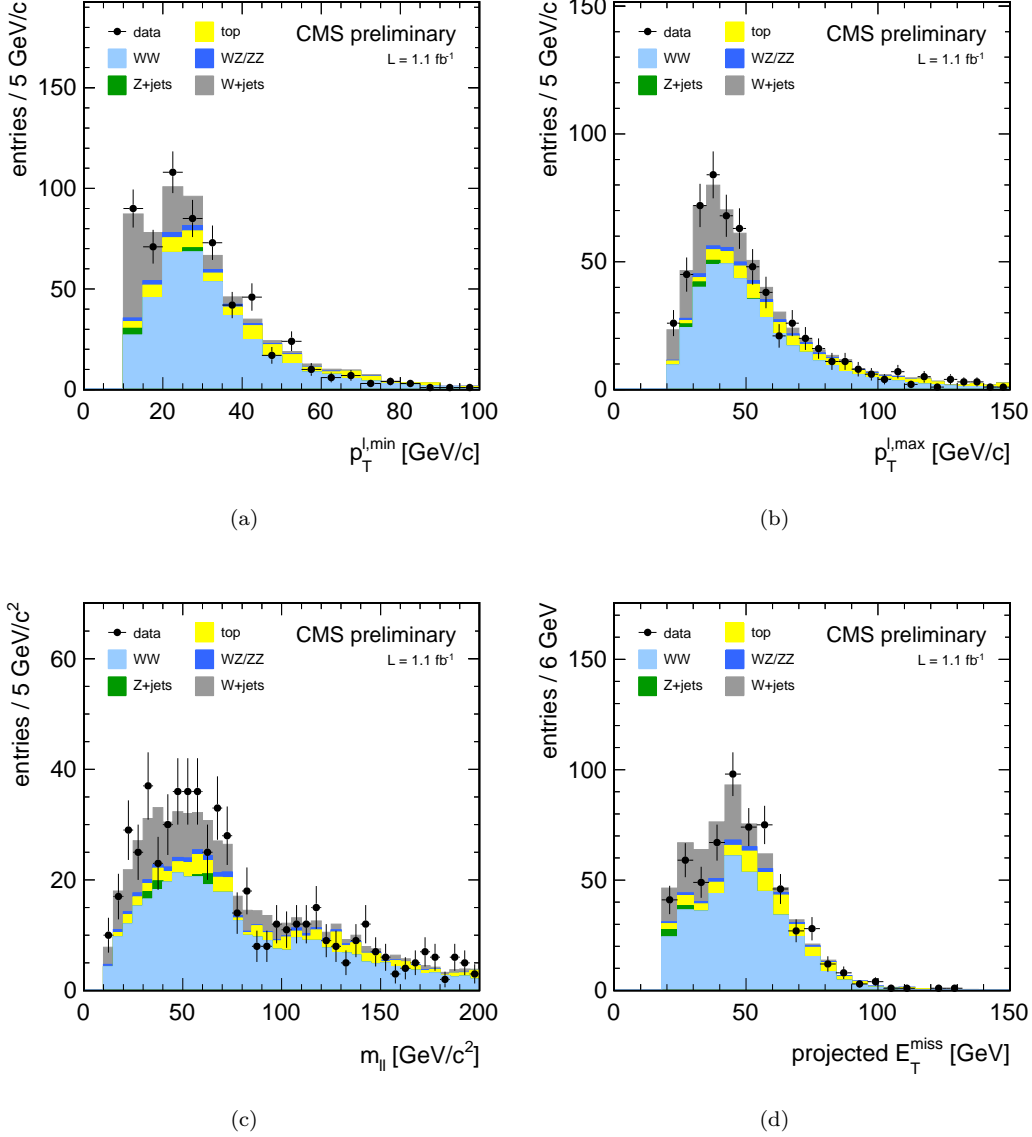


Figure 1: WW : Distributions of the trailing lepton p_T 1(a), leading lepton p_T 1(b), dilepton invariant mass 1(c) and the $\min(\text{proj}_{\text{MET}}, \text{proj}_{\text{trk-MET}})$. Each component in simulation is scaled to data-driven estimates.

- Veto events with one or more jets with $p_T > 30$ GeV to suppress the W +jets and top backgrounds. To further reduce the top quark background, apply a *top veto* based on soft-muon and b -jet tagging.
- Background contribution from ZZ and WZ diboson processes is reduced by rejecting events which have an additional third lepton passing identification and isolation requirements.

The above steps are described in detail in Ref. [3]. The backgrounds include: W + jets and QCD multi-jet events where at least one of the jets is misidentified as a lepton, top production ($t\bar{t}$ and tW), the $Z/\gamma^* \rightarrow \ell\ell$ process, and other diboson processes (WZ , ZZ and $W\gamma$). A combination of data-driven methods and detailed Monte Carlo (MC) simulation studies are used to estimate background contributions. The following backgrounds are estimated from data: W + jets, QCD, $Z/\gamma^* \rightarrow \ell\ell$, top, WZ and ZZ . The remaining background contributions, $W\gamma$ and $Z/\gamma^* \rightarrow \tau\tau$, are taken from simulation.

The total number of expected signal and background events, after applying the data-driven corrections, and observed data are reported in Table I. The distributions of the key analysis variables are shown in Figure 1. Systematic uncertainties are summarized in Table II. We obtain a total $W^+W^- \rightarrow 2\ell 2\nu$ efficiency of $(6.69 \pm$

Table I: Expected number of W^+W^- signal, and background events from the data-driven methods. Uncertainties include both statistical and systematic. Signal expectation is taken from simulation assuming NLO cross section.

Sample	Yield
$qq \rightarrow W^+W^-$	349.7 ± 30.3
$gg \rightarrow W^+W^-$	17.2 ± 1.6
$W + \text{jets}$	106.9 ± 38.9
$t\bar{t} + tW$	63.8 ± 15.9
$Z/\gamma^* \rightarrow \ell\ell + WZ + ZZ$	12.2 ± 5.3
$Z/\gamma^* \rightarrow \tau\tau$	1.6 ± 0.4
WZ/ZZ not in $Z/\gamma^* \rightarrow \ell\ell$	8.5 ± 0.9
$W + \gamma$	8.7 ± 1.7
signal + background	569 ± 52
Data	626

 Table II: Summary of main systematic uncertainties (relative, in %) in the W^+W^- cross section measurement.

Source	$qq \rightarrow W^+W^-$	$gg \rightarrow W^+W^-$	non-Z resonant WZ/ZZ	top	DY	$W + \text{jets}$	$V(W/Z) + \gamma$
Luminosity	—	—	6	—	—	—	6
Trigger efficiencies	1.5	1.5	1.5	—	—	—	1.5
Muon efficiency	1.5	1.5	1.5	—	—	—	1.5
Electron id efficiency	2.5	2.5	2.5	—	—	—	2.5
Momentum scale	1.5	1.5	1.5	—	—	—	1.5
E_T^{miss} resolution	2.0	2.0	2.0	—	—	—	1.0
pile-up	1.0	1.0	1.9	—	—	—	1.0
Jet counting	5.5	5.5	5.5	—	—	—	5.5
PDF uncertainties	3.0	3.0	4.0	—	—	—	4.0

0.51)%. The W^+W^- yield is calculated from the number of events in the signal region, after subtracting the expected contributions of the various SM background processes. From this yield and the $W \rightarrow \ell\nu$ branching fraction [4], the W^+W^- production cross section in pp collisions at $\sqrt{s} = 7$ TeV is found to be

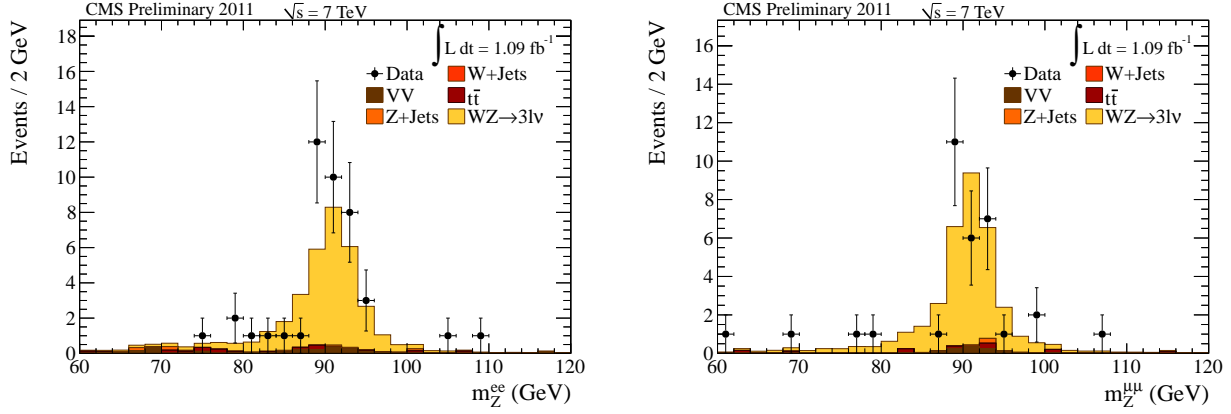
$$\sigma_{W^+W^-} = 55.3 \pm 3.3 (\text{stat}) \pm 6.9 (\text{syst}) \pm 3.3 (\text{lumi}) \text{ pb.}$$

This is consistent with the SM expectation of 43.0 ± 2.0 pb at NLO [5] within one standard deviation. More details on this measurement are given in Ref. [6].

4. Measurement of the $WZ \rightarrow \ell\nu\ell^+\ell^-$ cross section

The $WZ \rightarrow \ell\nu\ell^+\ell^-$ decay is characterized by a pair of same-flavor, opposite-charge isolated leptons with an invariant mass corresponding to the Z boson, together with a third isolated lepton and large E_T^{miss} . The background comes from events with 3 leptons, genuine or fake, and can be grouped in the following classes:

- Non-peaking background: di-lepton events without a Z boson, such as $t\bar{t}$, QCD or W +jets. All but the first of these can be neglected in this analysis.
- Events with Z + fake lepton, Z +jets (including Z +heavy quarks), or $Z\gamma$ (with photon conversion).
- Events with a real Z and a third isolated lepton, essentially from $ZZ \rightarrow 4\ell$ decays in which one of the four leptons is lost. This background is irreducible but is small due to the small ZZ cross section.

Figure 2: WZ : Dilepton invariant mass in the ee (left) and $\mu\mu$ (right) channels after all selection requirements.Table III: Observed and expected number of signal and background yields for the WZ events.

Sample	$3e0\mu$	$2e1\mu$	$1e2\mu$	$0e3\mu$
Z +Jets	0.89	0.10	0.31	0.17
$t\bar{t}$	0.83	0.95	0.56	0.59
$ZZ \rightarrow 4\ell$	0.40	0.95	0.40	0.97
$V\gamma$	0.80	0.10	0.03	0.00
W +Jets	0.00	0.00	0.00	0.00
$WW \rightarrow 2\ell 2\nu$ +Jets	0.02	0.04	0.00	0.00
Total Background	2.95	2.14	1.31	1.72
$WZ \rightarrow 3\ell\nu$	14.47	17.49	13.95	18.56
All MC	17.42	19.62	15.26	20.28
Data	22	20	13	20

Candidate events are selected using a double electron or double muon trigger. The Z boson is reconstructed from two opposite sign, same flavor leptons passing loose identification criteria. The leading and second leading lepton are required to have $p_T > 20(15)$ GeV and $p_T > 10(15)$ GeV for the $Z \rightarrow ee$ ($Z \rightarrow \mu\mu$) case, and their invariant mass should be in the range 60–120 GeV. In case of multiple candidates, the Z candidate with the mass closest to the nominal Z mass is selected. We look for the W boson decay by requiring a third isolated lepton with $p_T > 20$ GeV, and requiring E_T^{miss} in the event to be larger than 30 GeV.

The efficiency for leptons to pass the isolation and identification requirements is measured using “tag-and-probe” method from the Z events in data. The measured efficiency values for muons and electrons are 97% and 94%, respectively. In a data sample corresponding to $L = 1.1 \text{ fb}^{-1}$, 75 events pass these selection criteria. The data yield and MC expectations for each channel are given in Table III. The invariant mass of the Z candidates for the selected events is shown in Fig. 2. We estimate the Z +jets background using the data sidebands, and the fake-lepton originated backgrounds by computing the jet \rightarrow lepton fake rate from W +jets events in data. Similarly, we estimate the $t\bar{t}$ background contamination within the signal region using $t\bar{t}$ di-lepton events in data. We estimate all other background contributions, including $ZZ \rightarrow 4\ell$, $Z\gamma$, and $WZ \rightarrow l^+l'^-\nu_l\nu_{l'}$, where either ℓ or $\ell' = \tau$ from simulation.

The value of acceptance \times efficiency is 19% for the eee and $\mu\mu e$ final states each, 23% for the $ee\mu$ final state, and 25% for the $\mu\mu\mu$ final state. A summary of systematic uncertainties is given in Table IV. The cross sections for the four channels are combined, taking into account the correlations among the systematic uncertainties and known branching ratios [4]. This results in the cross section measurement

$$\sigma(pp \rightarrow WZ + X) = 17.0 \pm 2.4 \text{ (stat.)} \pm 1.1 \text{ (syst.)} \pm 1.0 \text{ (lumi.) pb.}$$

The theoretical NLO prediction is 19.79 ± 0.09 [5], which is in good agreement with the measured value. Cross section measurements in the individual channels are consistent with the central value. More details on this measurement are given in Ref. [6].

Table IV: Summary of systematic uncertainties in the $WZ \rightarrow 3\ell$ cross section measurement.

		eee	$ee\mu$	$\mu\mu e$	$\mu\mu\mu$
Source	Systematic uncertainty	Effect on $\mathcal{F} = A \cdot \epsilon_{MC}$			
Electron energy scale	2%	1.7%	0.25%	0.9%	n/a
Muon p_T scale	1%	n/a	0.5%	0.2%	0.9%
MET Resolution		0.5%	0.5%	0.5%	0.5%
MET Scale		0.3%	0.2%	0.1%	0.1%
Pileup		3.1%	0.8%	1.6%	1.6%
PDF	1.0%	1.0%	1.0%	1.0%	1.0%
NLO effect	2.5%	2.5%	2.5%	2.5%	2.5%
Total uncertainty on $\mathcal{F} = A \cdot \epsilon_{MC}$		4.5%	2.9%	3.3%	3.3%
Source	Systematic uncertainty	Effect on ρ_{eff}			
Electron trigger	1.5%	1.5%	1.5%	n/a	n/a
Electron reconstruction	0.9%	2.7%	1.8%	0.9%	n/a
Electron ID and isolation	2.5% (loose), 3.2% (tight)	5.9%	5.0%	3.2%	n/a
Muon trigger	0.54%	n/a	n/a	1.08%	1.08%
Muon reconstruction	0.74%	n/a	0.74%	1.48%	2.22%
Muon ID and isolation	0.74%	n/a	0.74%	1.48%	1.94%
Total uncertainty on ρ_{eff}		6.7%	5.6%	4.2%	3.6%
Source	Systematic uncertainty	Effect on WZ yield			
Background estimation					
ZZ	7.5%	0.2%	0.4%	0.3%	0.4%
$Z\gamma$	13%	0.5%	0.08%	0.04%	0.08%
$t\bar{t}$		1.3%	1.3%	0.9%	0.5%
Jet fake rate		3.3%	4.9%	5.2%	4.2%
Source	Systematic uncertainty	Effect on luminosity			
Luminosity	6.0%	6.0%	6.0%	6.0%	6.0%

5. Measurement of the $ZZ \rightarrow \ell^+\ell^-\ell^+\ell^-$ cross section

The $ZZ \rightarrow \ell^\pm\ell^\mp\ell'^\pm\ell'^\mp$ process with $\ell, \ell' = e, \mu$, or τ is characterized by two pairs of same flavor, opposite charge, high p_T , isolated leptons, coming from the primary vertex, with an invariant mass corresponding to a Z boson. The process has a clean signature with very little experimental background. We reconstruct each Z boson in the mass range $60 < m_Z < 120$ GeV. One Z is required to decay into a pair of electrons or muons, and the second Z can decay to $\mu\mu, ee$ or $\tau\tau$. The data sample used for this analysis corresponds to $\mathcal{L} = 1.1 \text{ fb}^{-1}$, and most of the events are selected using a double electron or double muon trigger. For the 4ℓ final state with $\ell = e, \mu$, we require the following event selection:

1. *First Z*: a pair of loosely identified lepton candidates of opposite charge and matching flavor (e^+e^- , $\mu^+\mu^-$) satisfying $m_{1,2} > 60$ GeV, $p_{T,1} > 20$ GeV and $p_{T,2} > 10$ GeV; the pair with reconstructed mass closest to the nominal Z boson mass is retained.
2. *Choice of the “best 4ℓ ”*: retain a second lepton pair of opposite charge and matching flavor, among all the remaining $\ell^+\ell^-$ combinations with $60 < m_Z < 120$ GeV and such that the reconstructed four-lepton invariant mass satisfies $m_{4\ell} > 100$ GeV. If more than one combination is found satisfying all the criteria, the one built from leptons of highest p_T is chosen.

For the $2\ell 2\tau$ final state, the first Z boson is required to decay to $\mu\mu$ or ee as described above, and the second Z decays into a pair of taus. Each tau candidate can decay leptonically to a μ or e , or hadronically. Therefore, there are four possible final states for the second Z : $\mu\tau, e\tau, \tau\tau, \mu e$. The selection requirements are:

- Muon or electron with p_T greater than 10 GeV, hadronic taus with p_T greater than 20 GeV;
- The two leptons should be isolated and should have opposite charge.

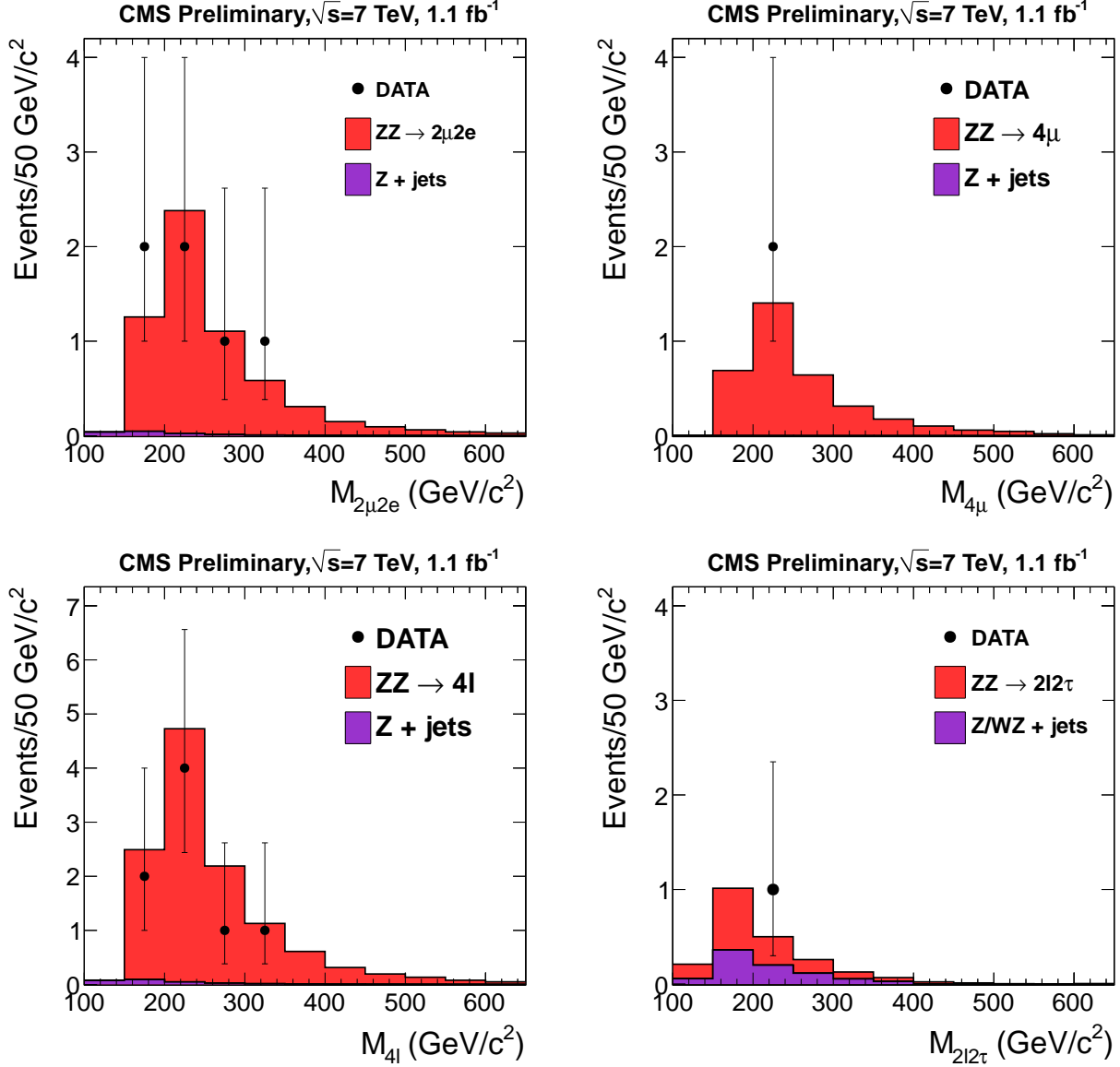


Figure 3: ZZ : Distributions of the four-lepton reconstructed mass for the $2e2\mu$ and the 4μ final states (top). No events were observed in the $4e$ final state. The bottom left plot represents the sum of the three 4ℓ channels. The bottom right plot shows the invariant mass of the $2l2\tau$ final state. The data samples correspond to $L = 1.1 \text{ fb}^{-1}$.

- $30 \leq \text{Visible Mass} (ll) \leq 80 \text{ GeV}$

The reducible instrumental background is very small or negligible. We estimate any residual background and the associated systematic uncertainty using empirical methods based on experimental data. These are described in more detail in Ref. [6]. In the 4ℓ final state, we observe $N_{\text{obs}} = 8$ events compared to 12.5 ± 1.1 events expected from the SM. The reconstructed four-lepton invariant mass distribution is shown in Fig. 3. Table V shows the number of expected and observed events for the individual final states, and also the number of background events estimated using data-driven techniques. The main sources of systematic uncertainties are summarized in Table VI. The acceptance for the kinematic thresholds and detector coverage is in the range 0.56–0.59 for the 4μ , $4e$ and $2e2\mu$, and 0.18–0.21 for the $2l2\tau$ final states. The resulting cross section is

$$\sigma(pp \rightarrow ZZ + X) = 3.8^{+1.5}_{-1.2}(\text{stat.}) \pm 0.2(\text{sys.}) \pm 0.2(\text{lumi.}) \text{ pb},$$

Table V: Number of expected and observed events for the individual ZZ final states.

Final state	N_{observed}	$N_{\text{estimated}}^{\text{backg.}}$	N_{expected}^{ZZ}
4μ	2	0.004 ± 0.004	3.7 ± 0.4
$4e$	0	0.14 ± 0.06	2.5 ± 0.2
$2e2\mu$	6	0.15 ± 0.06	6.3 ± 0.6
$2l2\tau$	1	0.8 ± 0.1	1.4 ± 0.1

 Table VI: Summary of statistical and systematic uncertainties in the $ZZ \rightarrow \ell^+ \ell^- \ell^+ \ell^-$ cross section measurement.

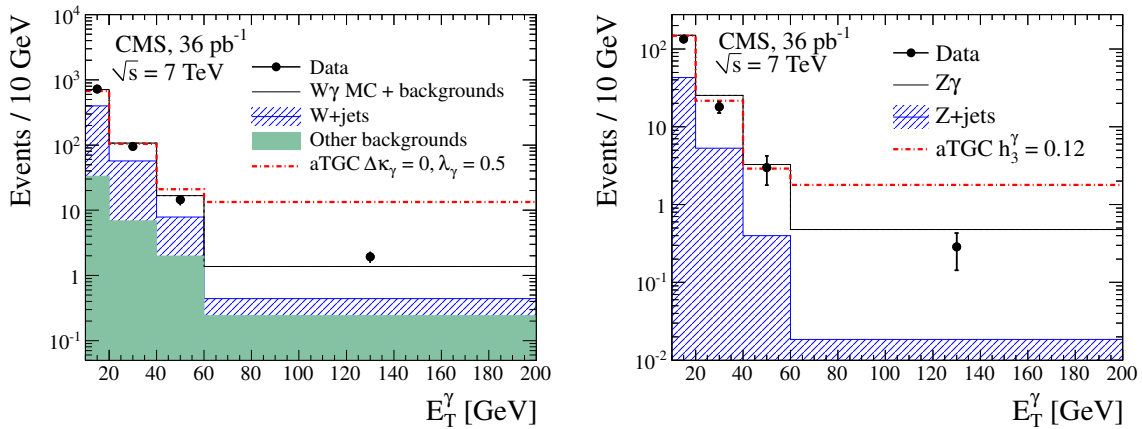
	4μ	$4e$	$2e2\mu$
source	Effects on acceptance A		
PDF+QCD scale	2.2 %	2.2 %	1.8 %
source	Effects on efficiency ϵ		
total uncertainty on ϵ	1.7 %	3.7 %	3.0 %
Background (Z+jets)	100 %	43 %	40 %
Luminosity	6 %		

which can be compared to the theoretical NLO prediction 6.4 ± 0.6 pb computed with MCFM [5]. More details on this measurement are given in Ref. [6].

6. Measurements of the $W\gamma$ and $Z\gamma$ cross sections

The $W\gamma \rightarrow \ell\nu\gamma$ final state is characterized by a prompt, energetic, and isolated lepton, significant E_T^{miss} due to the presence of the neutrino from the W boson decay, and a prompt isolated photon. The $Z\gamma \rightarrow \ell\ell\gamma$ final state has two isolated leptons and a prompt isolated photon. Data for this study are selected with a trigger that requires at least one energetic electron or muon. This requirement is about 90% efficient for the $W\gamma \rightarrow \mu\nu\gamma$ signal and 98% efficient for $W\gamma \rightarrow e\nu\gamma$. The trigger efficiency is close to 100% for both $Z\gamma \rightarrow \ell\ell\gamma$ final states. As the $W\gamma$ and $Z\gamma$ cross sections diverge for soft photons or, in the case of $Z\gamma$ production, for small values of the dilepton invariant mass, we restrict the cross section measurement to the phase space defined by photon $E_T > 10$ GeV and $\Delta R(\ell, \gamma) > 0.7$. Furthermore, for $W\gamma$ the E_T^{miss} in the event must exceed 25 GeV, and for the $Z\gamma$ the $m_{\ell\ell}$ must be above 50 GeV. The data sample used for this analysis corresponds to $L = 36 \text{ pb}^{-1}$.

We require a well identified and isolated photon candidate in $|\eta| < 1.44$ or $1.57 < |\eta| < 2.5$. The isolated


 Figure 4: $W\gamma$, $Z\gamma$: Transverse energy distribution of the photon candidate (left: $W\gamma$, right: $Z\gamma$).

leptons from the W or Z decay are required to have $p_T > 20$ GeV and $|\eta| < 2.5$ (2.4 for muon). The muon candidate in $W\gamma \rightarrow \mu\nu\gamma$ is further restricted to be in $|\eta| < 2.1$. The main background to $W\gamma/Z\gamma$ production comes from W/Z +jets processes. We estimate this in data by measuring the E_T -dependent probability for a jet to be identified as photon, and then folding this probability with the non-isolated photon candidate E_T spectrum. The E_T distribution for photon candidates in events passing the full selection is given in Fig. 4. For $W\gamma$, we observe 452 events in the $e\nu\gamma$ and 520 events in the $\mu\nu\gamma$ final states. The background from misidentified jets is estimated to be 220 ± 16 (stat.) ± 14 (syst.) for $e\nu\gamma$, and 261 ± 19 (stat.) ± 16 (syst.) for $\mu\nu\gamma$. Backgrounds from other sources, such as $Z\gamma$ and diboson, are estimated from simulation and found to be 7.7 ± 0.5 and 16.4 ± 1.0 for $W\gamma \rightarrow e\nu\gamma$ and $W\gamma \rightarrow \mu\nu\gamma$, respectively. The process $W\gamma \rightarrow \tau\nu\gamma$, with subsequent $\tau \rightarrow \ell\nu\nu$ decay, also contributes at the percent level and is estimated from simulation. For $Z\gamma$, we observe 81 events in the $ee\gamma$ and 90 events in the $\mu\mu\gamma$ final states. The Z +jets background to these final states is estimated to be 20.5 ± 1.7 (stat.) ± 1.9 (syst.) and 27.3 ± 2.2 (stat.) ± 2.3 (syst.), respectively. Other backgrounds are negligibly small. All systematic uncertainties are summarized in Table VII.

Leading order $W\gamma$ production can be described by three processes: initial state radiation (ISR), where a photon is radiated by one of the incoming quarks; final state radiation (FSR), where a photon is radiated from the charged lepton from the W boson decay; and finally through the $WW\gamma$ vertex, where a photon couples directly to the W boson. The three tree-level $W\gamma$ production processes interfere with each other, resulting in a radiation-amplitude zero (RAZ) in the angular distribution of the photon. In the SM, the location of the dip minimum is located at $Q_\ell \times \Delta\eta = 0$. Anomalous $W\gamma$ production can result in a flat distribution. In Fig. 5 we plot the charge-signed rapidity difference in background-subtracted data. There is a good agreement between the data and MC prediction. In the SM, leading order $Z\gamma$ production is described via ISR and FSR processes only, because the $ZZ\gamma$ and $Z\gamma\gamma$ TGCs are not allowed at the tree level. The distribution of the $\ell\ell\gamma$ mass as a function of the dilepton mass is shown in Fig. 5.

Table VII: Summary of systematic uncertainties in $W\gamma$ and $Z\gamma$ cross section measurements.

	$W\gamma \rightarrow e\nu\gamma$	$W\gamma \rightarrow \mu\nu\gamma$	$Z\gamma \rightarrow ee\gamma$	$Z\gamma \rightarrow \mu\mu\gamma$
Source	Effect on $A \cdot \epsilon_{MC}$			
Lepton energy scale	2.3%	1.0%	2.8%	1.5%
Lepton energy resolution	0.3%	0.2%	0.5%	0.4%
Photon energy scale	4.5%	4.2 %	3.7%	3.0%
Photon energy resolution	0.4%	0.7%	1.7%	1.4%
Pile-up	2.7%	2.3%	2.3%	1.8%
PDFs	2.0%	2.0%	2.0%	2.0%
Total uncertainty on $A \cdot \epsilon_{MC}$	6.1%	5.2%	5.8%	4.3%
	Effect on $\epsilon_{data}/\epsilon_{MC}$			
Trigger	0.1%	0.5%	< 0.1%	< 0.1%
Lepton identification and isolation	0.8%	0.3%	1.1%	1.0%
E_T^{miss} selection	0.7%	1.0%	N/A	N/A
Photon identification and isolation	1.2%	1.5%	1.0%	1.0%
Total uncertainty on $\epsilon_{data}/\epsilon_{MC}$	1.6%	1.9%	1.6%	1.5%
Background	6.3%	6.4%	9.3%	11.4%
Luminosity	4%			

We find the cross section for $W\gamma$ production to be $\sigma(\text{pp} \rightarrow W\gamma + X) \times \mathcal{B}(W \rightarrow e\nu) = 57.1 \pm 6.9$ (stat.) ± 5.1 (syst.) ± 2.3 (lumi.) pb and $\sigma(\text{pp} \rightarrow W\gamma + X) \times \mathcal{B}(W \rightarrow \mu\nu) = 55.4 \pm 7.2$ (stat.) ± 5.0 (syst.) ± 2.2 (lumi.) pb. The combination of the two results yields $\sigma(\text{pp} \rightarrow W\gamma + X) \times \mathcal{B}(W \rightarrow \ell\nu) = 56.3 \pm 5.0$ (stat.) ± 5.0 (syst.) ± 2.3 (lumi.) pb. This result agrees well with the NLO prediction [7] of 49.4 ± 3.8 pb. The $Z\gamma$ cross section is measured to be $\sigma(\text{pp} \rightarrow Z\gamma + X) \times \mathcal{B}(Z \rightarrow ee) = 9.5 \pm 1.4$ (stat.) ± 0.7 (syst.) ± 0.4 (lumi.) pb for the $ee\gamma$ final state, and $\sigma(\text{pp} \rightarrow Z\gamma + X) \times \mathcal{B}(Z \rightarrow \mu\mu) = 9.2 \pm 1.4$ (stat.) ± 0.6 (syst.) ± 0.4 (lumi.) pb for the $\mu\mu\gamma$ final state. The combination of the two results yields $\sigma(\text{pp} \rightarrow Z\gamma + X) \times \mathcal{B}(Z \rightarrow \ell\ell) = 9.4 \pm 1.0$ (stat.) ± 0.6 (syst.) ± 0.4 (lumi.) pb. The theoretical NLO prediction [8] is 9.6 ± 0.4 pb, which is in agreement with the measured value. More details on these measurements are given in Ref. [9].

Table VIII: One dimensional 95% CL limits on WWZ , $WW\gamma$, $ZZ\gamma$, and $Z\gamma\gamma$ aTGCs.

WWZ	$WW\gamma$	$ZZ\gamma$	$Z\gamma\gamma$
$-0.19 < \lambda_Z < 0.19$	$-0.61 < \Delta\kappa_\gamma < 0.61$	$-0.05 < h_3 < 0.06$	$-0.07 < h_3 < 0.07$
$-0.29 < \Delta g_1^Z < 0.31$	$-0.18 < \lambda_\gamma < 0.17$	$-0.0005 < h_4 < 0.0005$	$-0.0005 < h_4 < 0.0006$

7. Limits on anomalous triple gauge couplings from 36 pb^{-1} data

The most general Lorentz-invariant Lagrangian that describes the $WW\gamma$ coupling has seven independent dimensionless couplings g_1^γ , κ_γ , λ_γ , g_4^γ , g_5^γ , $\tilde{\kappa}_\gamma$, and $\tilde{\lambda}_\gamma$ [4]. By requiring CP invariance and $SU(2) \times U(1)$ gauge invariance only two independent parameters remain: κ_γ and λ_γ . From WWZ coupling introduces two more independent parameters: λ_Z and g_1^Z . In the SM, $\kappa_\gamma = 1$, $g_1^Z = 1$, $\lambda_\gamma = 0$, and $\lambda_Z = 0$. We define anomalous TGC (aTGCs) to be deviations from the SM predictions, so instead of using κ_γ we define $\Delta\kappa_\gamma \equiv \kappa_\gamma - 1$. For the $ZZ\gamma$ or $Z\gamma\gamma$ couplings, the most general Lorentz-invariant and gauge-invariant vertex is described by only four parameters h_i^V ($i = 1, 2, 3, 4$; $V = \gamma, Z$) [8]. By requiring CP invariance, only two parameters, h_3^V and h_4^V , remain. The SM predicts these couplings to vanish at tree level. We produce simulated samples of WW , $W\gamma$ and $Z\gamma$ signals for a wide range of aTGCs values. A grid of λ_γ and $\Delta\kappa_\gamma$ values is used for the $WW\gamma$ coupling, λ_Z and $g_1^Z = 1$ values for the WWZ coupling, and h_3 and h_4 values for the $ZZ\gamma$ and $Z\gamma\gamma$ couplings.

Assuming Poisson statistics and log-normal (Gaussian in case of WW) distributions for the generated samples and background systematic uncertainties we calculate the likelihood of the observed photon E_T (for $W\gamma$, $Z\gamma$ samples) or the leading lepton p_T (in case of WW sample) spectrum in data given the sum of the background and aTGCs predictions for each point in the grid of aTGCs values. The resultant two-dimensional 95% confidence level (CL) limits are given in Fig. 6 and in Fig. 7. To set one-dimensional 95% CL limits on a given anomalous coupling we set the other aTGCs to their respective SM predictions. The results are summarized in Table VIII. Figure 8 shows the leading lepton p_T distributions in data and the predictions for the SM WW signal and background processes, and for a set of large anomalous couplings. All the non-SM terms in the effective Lagrangian are scaled with α/m_V^n , where α is an aTGC, m_V is the mass of the gauge boson (W boson for the $WW\gamma$ coupling, and Z boson for $ZZ\gamma$ and $Z\gamma\gamma$ couplings), and n is a power that is chosen to make the aTGC dimensionless. The values of n for $\Delta\kappa_\gamma$, λ_γ , h_3 , and h_4 are 0, 2, 2, and 4, respectively. An alternative way to scale those new physics Lagrangian terms is with $\alpha/\Lambda_{\text{NP}}^n$, where Λ_{NP} is the characteristic energy scale of new physics. We present upper limits on aTGCs for Λ_{NP} values between 2 and 8 TeV in Fig. 8.

More details on these measurements are given in Ref. [9] and Ref. [3].

References

- 1 R. Adolphi *et al.*, CDF Collaboration, JINST **3**, S08004 (2008).
- 2 S. Chatrchyan *et al.* [CMS Collaboration], Phys. Lett. B **699**, 25 (2011).
- 3 CMS Collaboration, “Search for the Higgs Boson in the Fully Leptonic W^+W^- Final State”, CMS-PAS-HIG-11-014, url: <http://cdsweb.cern.ch/record/1376638?ln=en> (2011).
- 4 K. Nakamura *et al.* (Particle Data Group), J. Phys. **G 37**, 075021 (2010).
- 5 J. Campbell, K. Ellis, and C. Williams, “MCFM - Monte Carlo for FeMtobarn processes”, url: <http://mcfm.fnal.gov> (2011).
- 6 CMS Collaboration, “Measurement of the WW , WZ and ZZ cross sections at CMS”, CMS-PAS-EWK-11-010, url: <http://cdsweb.cern.ch/record/1370067?ln=en> (2011).
- 7 U. Baur, T. Han, and J. Ohnemus, Phys. Rev. **D48**, 5140 (1993).
- 8 U. Baur and E. Berger, Phys. Rev. **D47**, 4889 (1993).
- 9 S. Chatrchyan *et al.* [CMS Collaboration], Phys. Lett. B **701**, 535 (2011).

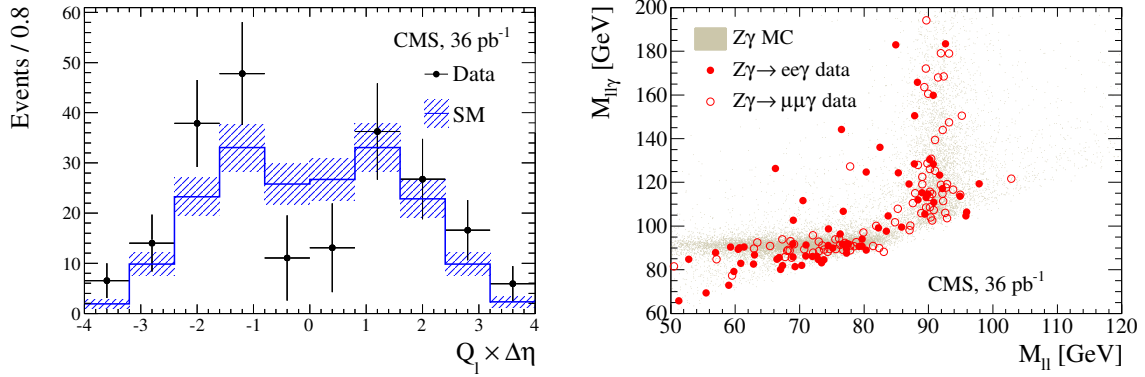


Figure 5: $W\gamma$, $Z\gamma$: (left) Charge-signed rapidity difference in the $W\gamma$ production (electron and muon channels combined). (right) Distribution of the $\ell\ell\gamma$ invariant vs. $\ell\ell$ invariant mass for the $Z\gamma$ candidates. The data accumulation at $M_{\ell\ell\gamma} \simeq M_Z$ corresponds to FSR events, while the data at $M_{\ell\ell} \simeq M_Z$ correspond to ISR events.

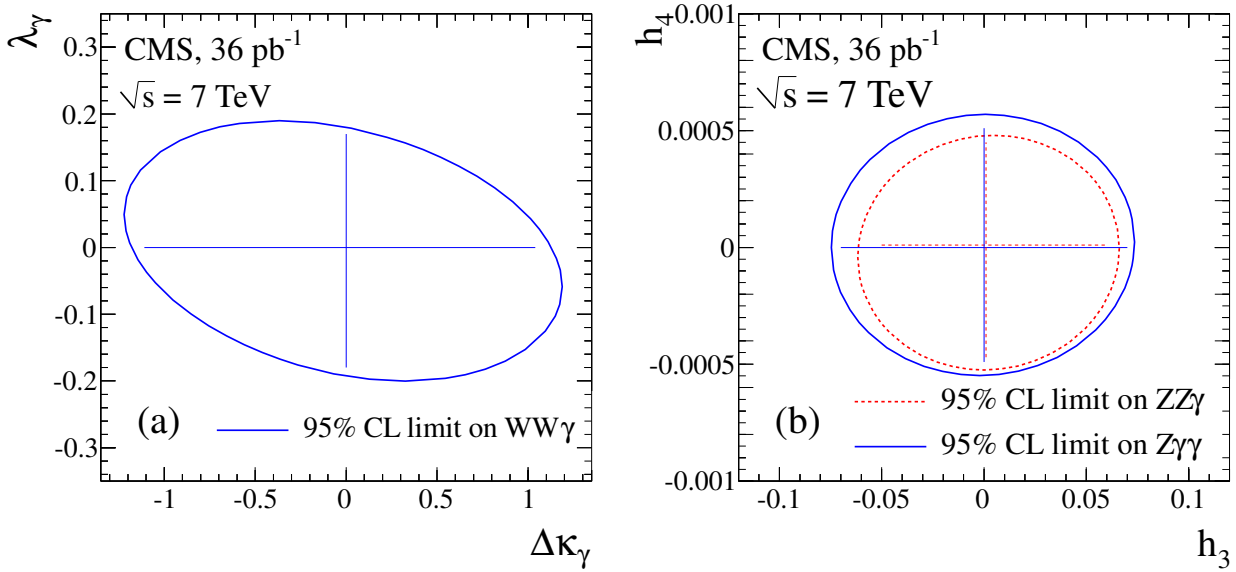


Figure 6: Two-dimensional 95% CL limit contours (a) for the $WW\gamma$ vertex couplings λ_γ and $\Delta\kappa_\gamma$ (blue line), and (b) for the $ZZ\gamma$ (red dashed line) and $Z\gamma\gamma$ (blue solid line) vertex couplings h_3 and h_4 assuming no energy dependence on the couplings. One-dimensional 95% CL limits on individual couplings are given as solid lines.

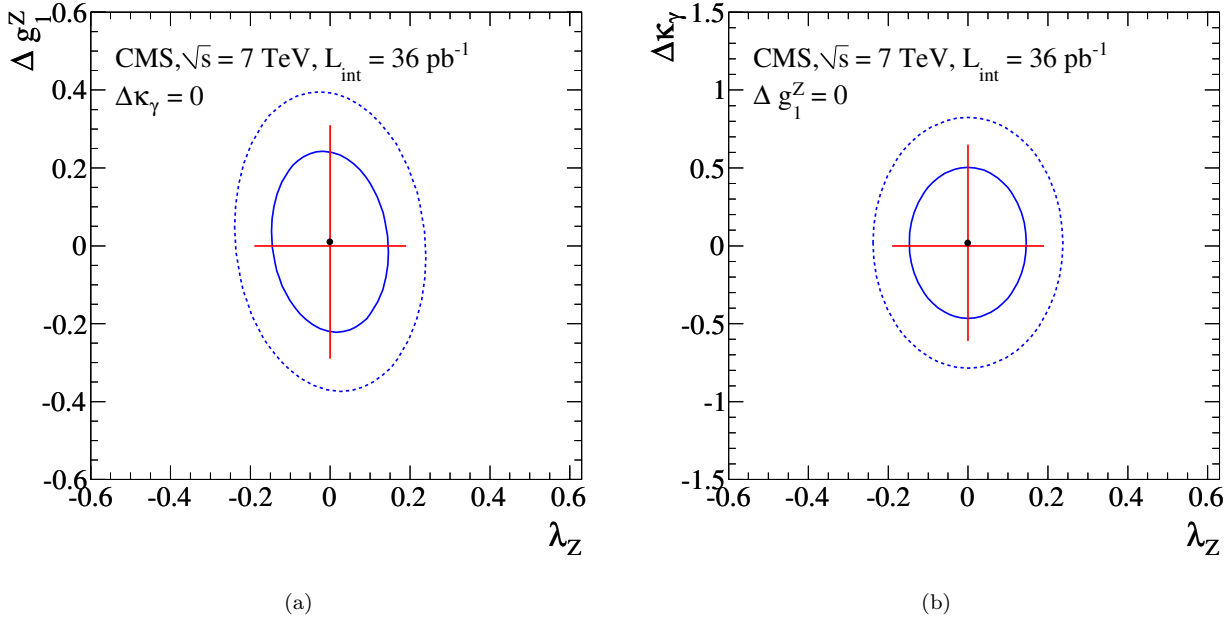


Figure 7: 68% (solid blue lines) and 95% CL (dotted blue lines) as well as the central value (point) and one-dimensional 95% CL limits (red lines) derived from WW events for (a) $\Delta \kappa_\gamma = 0$ and (b) $\Delta g_1^Z = 0$.

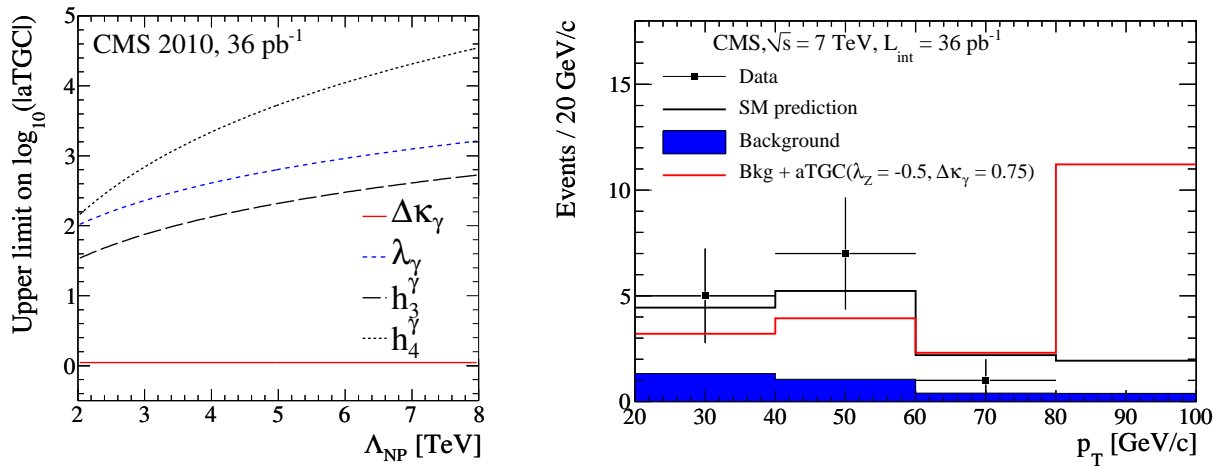


Figure 8: (left) Upper 95% CL limits on $\log_{10}(|aTGC|)$ as a function of Λ_{NP} for $\Delta \kappa_\gamma$, λ_γ , h_3^γ , and h_4^γ . Limits on the latter two couplings are similar to those for h_3^Z and h_4^Z . These limits refer to the formulation in which the new physics Lagrangian terms are scaled with $\alpha/\Lambda_{\text{NP}}^n$, where Λ_{NP} is the characteristic energy scale of new physics and α is the aTGC. (right) Leading lepton p_T distribution in WW data overlaid with predictions from the SM simulation, background only simulation (Bkg in the figure), and the simulation with large anomalous couplings ($aTGC$ in the figure).